

Chapter 14

Remote Sensing of Coastal Mangrove Forest

Le Wang and Wayne P. Sousa

Mangroves, once occupied 75% of the world's tropical and subtropical coastlines, are seriously threatened by coastal development projects and accelerated climate change, e.g. sea-level rise. In this study, we aim to attain three objectives: (1) to develop effective methods for discriminating mangrove species from IKONOS imagery; (2) to determine an optimal season for capturing the spectral and textural difference among mangrove species; (3) to investigate the capability of hyperspectral data for distinguishing mangrove species. Our study site is in Panama. Two scenes of IKONOS imagery respectively acquired during dry and wet seasons were employed. A Clustering-Based Neural Network (CBNN) classifier was developed and its performance was compared with two other conventional classifiers: Back-Propagation Neural Networks classifier (BPNN) and Maximum Likelihood Classifier (MLC). Results indicate that CBNN is superior to BPNN and MLC in employing textural information. Rainy season is better than dry season for mangrove species classification. To investigate the third objective, a one-way ANNOVA followed by linear discriminate analysis (LDA) method was devised for analyzing the leaf-level hyperspectral reflectance. A kappa value of 0.9 was achieved in classifying leaves from three species. Four narrow-band indices were tested for detecting stress conditions associated with the three mangrove species.

14.1 Introduction

Mangrove forests are highly productive ecosystems that typically dominate the intertidal zone of low energy tropical and subtropical coastlines (Lugo and Snedaker 1974, Kathiresan and Bingham 2001). The constituent species in these forests are often differentially distributed with distance from the water's edge, forming zones of differing species composition perpendicular to the intertidal gradient. Mangrove habitats and the organisms they support are of significant ecological and economic value (Lugo and Snedaker 1974, Tomlinson 1986, Hutchings and Saenger 1987,

L. Wang (✉)

Department of Geography, State University of New York at Buffalo, Buffalo, NY 14261, USA
e-mail: lewang@buffalo.edu

Hogarth 1999, Kathiresan and Bingham 2001). Among other values, mangroves (1) provide vital habitat for a wide variety of animal and plants species, many of them uniquely adapted to mangrove environments, and some of them rare and/or endangered, (2) function as nursery and feeding grounds for many species of commercially valuable fishes, crustaceans, and molluscs, (3) are an important source of carbon to detritus-based food webs in adjacent coastal waters, (4) stabilize deposited sediments, reducing shoreline erosion, (5) buffer the impact of storm waves and floods on inland areas, and (6) trap nutrients and sediments in runoff from upland areas, helping to maintain the quality of estuarine and nearshore waters.

However, mangrove forests' health and persistence are seriously threatened by coastal development projects and various forms of non-renewable exploitation (Saenger et al. 1983, Ellison and Farnsworth 1996, Farnsworth and Ellison 1997). In recent decades, mangrove habitats have suffered dramatic declines in area (Saenger et al. 1983, Farnsworth and Ellison 1997, Ellison and Farnsworth 2001, Alongi 2002) due to coastal development, non-renewable resource exploitation (e.g. clear cutting, mining, aquaculture), pollution, high rates of sedimentation, and alterations of hydrology. Alongi (2002) estimated that as much as a third of the world's mangrove forest have been lost in the past 50 years. In the Caribbean, the rate of mainland mangrove deforestation is estimated to be 1.4–1.7% annually (Ellison and Farnsworth 1996, FAO 2003), comparable to the rates documented for threatened tropical rainforests. Thus, there is an increasing need to monitor and assess mangrove forest structure and dynamics, both to gain a better understanding of their basic biology and to help guide conservation and restoration efforts. The ability to accurately map mangrove species with the tools of remote sensing would greatly assist in this effort.

Although remote sensing has been used to map many of the land cover types on earth, it has not been widely used for mapping mangrove forests due to the limited spectral and spatial resolution with conventional imagery. Using the conventional multispectral remote sensing imagery, study has been concentrated on distinguishing mangrove from non-mangrove habitats, without regard to species of mangrove. Among these studies, Venkataratnam and Thammappa (1993) used Landsat Multispectral Scanner (MSS) data to map mangroves along the coastline of Andhra Pradesh, India. Rasolofoharino et al. (1998) produced a detailed cartographic inventory of a mangrove ecosystem in Madagascar based on a classification from Satellite pour l'Observation de la Terre (SPOT) images (SPOT 1 and 2). Gao (1998) developed a two-tiered classification scheme based on a SPOT image and applied it to the mangrove mapping in the Waitemata Harbour of Auckland, New Zealand. This method was 81.4% accurate in classifying mangrove versus non-mangrove land cover. Green et al. (1998) compared the suitability of three types of data (SPOT XS, Landsat TM, CASI) in mapping mangrove species with five different classification approaches. Gao (1999) conducted a comparative study on mangrove mapping with SPOT XS and Landsat Thematic Mapper (TM) images at 10, 20, 30 m resolution.

Given the small patch size of some mangrove species, spatial resolution plays a more important role than spectral resolution in discriminating different mangrove species. The recent launching of so-called "Very High Resolution" (VHR) satellite sensors provides a new opportunity to map land cover types at a much higher

spatial resolution than with previously available sensors. In the VHR category, there are two major commercial sources of imagery: IKONOS images and QuickBird images. The IKONOS 2 satellite, launched in 1999, provided the first publically available VHR satellite images, while even higher resolution images became available from the QuickBird satellite in 2001. With this enhanced spatial resolution, a better classification of individual mangrove species has become possible. However, another challenge emerged, which is to develop analytical approaches that can realize the full potential of the acquired data when attempting to define and discriminate spatial entities. The development of methods for mapping mangrove forests using information collected by high resolution sensors, particularly at the species-level, is still at an early exploratory stage. Mumby and Edwards (2002) were able to improve thematic accuracy for a marine environment comprised of 13 habitat classes (including mangroves) by incorporating texture information in their analysis of an IKONOS image. Held et al. (2003) employed an integrated analysis of data from the high spatial/spectral resolution scanner CASI and the airborne AIRSAR (NASA's polarimetric radar) to map mangrove estuaries along the Daintree River in North Queensland, Australia. Higher classification accuracies of different habitats and mangrove forest types were achieved when hyperspectral and radar data were used in combination, and a slight improvement (around 3%) was achieved using a hierarchical neural network in place of MLC. Wang et al. (2004a) developed an integrated pixel-based and object-based method, and achieved a moderately accurate result when classifying the canopies of three mangrove species in an IKONOS image. Furthermore, Wang et al. (2004b) compared the ability to discriminate the canopies of different mangrove species using various combinations of spectral and textural information inherent to IKONOS and QuickBird imagery.

This chapter investigated effective methods that can be employed for monitoring and assessing the spatial and temporal pattern of mangrove forests with images acquired from VHR satellite sensors as well as hyperspectral sensors. Specifically, the following objectives are to be attained: (1) to investigate and develop suitable methods for discriminating mangrove species; (2) to determine an optimal season for capturing the spectral difference among mangrove species; (3) to investigate the capability of hyperspectral data for distinguishing mangrove species.

14.2 Study Sites

The study was conducted in mainland mangrove forests near the Smithsonian Tropical Research Institute's Galeta Marine Laboratory ($9^{\circ}24'18''\text{N}$, $79^{\circ}51'48.5''\text{W}$) at Punta Galeta on the Caribbean coast of Panama, approximately 8 km northeast of the city of Colon.

Three tree species comprise the canopy of the study forests. They are: black mangrove (*Avicennia germinans*), white mangrove (*Laguncularia racemosa*), and red mangrove (*Rhizophora mangle*). Red mangrove forms a pure or nearly pure stand at the seaward fringe. About 10–20 m from the water's edge, white mangrove joins the canopy, forming a nearly even mixture with red mangrove in the low intertidal.

In these mixed-species stands, white mangroves reach average heights of 22 m, while red mangroves average 16 to 18 m in height (W. Sousa, unpublished data). So, the crowns of white mangroves tend to be emergent, and therefore more visible in the satellite image than those of red mangroves, which form a lower sub-canopy. Black mangrove joins the canopy in the mid-intertidal, creating a mixed canopy of the three species, and then gradually monopolizes most upper intertidal stands. White mangrove may disappear completely from the canopy in the upper intertidal, or occur only as scattered individuals or small stands (W. Sousa, unpublished data).

Over the past 31 years, Punta Galeta has received, on average, 2781 mm of rainfall per year (based on measurements made at the Galeta Marine Laboratory by the Smithsonian Tropical Research Institute's Environmental Science Program). There is marked seasonality in precipitation, with more than 90% of rainfall occurring between early May and late December (Cubit et al. 1988, 1989, Duke et al. 1997). Aspects of mangrove phenology exhibit a strong association with seasonal rainfall patterns. We regularly observe that new leaves are flushed primarily during the wet season, and this pattern was quantified for *Rhizophora mangle* on Punta Galeta by Duke and Pinzón (1993). They found that leaf production was lowest from December to February (dry season) and peaked in May to July (early wet season). Since the spectral properties of leaves change as they age (Carter et al. 1989), we would expect canopy reflectance to change seasonally with the shift in average leaf age.

14.3 Mangrove Species Classification with High Spatial Resolution Imagery

14.3.1 Data Collection and Preprocessing

Two scenes of IKONOS Geo bundle images were employed in this study. They were acquired on 2 February 2004 at 16:04 pm local time and 8 May 2004 at 16:01 local time. Metadata for the two sets of images indicate that both were collected at a similar sensor elevation: 85.8° for the February images and 79.1° for the May images. The high elevation angle largely offsets the geometric distortion induced by variation in terrain elevation, which is very modest in mangrove habitats. An image to image registration was conducted using May imagery as the reference image and a registration error: root mean square (RMS) of 0.5 pixels was reported. A nearest neighbor resampling approach was adopted to rectify the February image.

14.3.2 Methodology

14.3.2.1 Back-Propagation Neural Networks Classifier (BPNN)

A BPNN is a multi-layered feed-forward network trained by the so-called back-propagation algorithm as first introduced by Rumelhart et al. (1986). This learning

algorithm, also called the generalized delta rule, is an iterative gradient descent training procedure. It is carried out in two stages. In the first stage, once the network weights have been randomly initialized, the input data are presented to the network and propagated forward to estimate the output value for each training pattern set. In the second stage, the difference (error) between known and estimated outputs is minimized. The whole process is repeated, with weights being recalculated at each iteration, until the error is minimal, or lower than a given threshold. For the classification problem a BPNN classifier recognizes spectral patterns by learning from training sets. After training, the neural network system fixes all the weights and maintains the original learning parameters. The classification process calculates the output of each pixel using the parameters learned from the training phase, and then decides the class assignment of the pixel.

In this study, a BPNN with two hidden layers of 24 and 12 neurons respectively, hereafter referred to as BP:24:12, was trained using the MATLAB Neural Network Toolbox (V4.0.2-R13). One input node per band and one output neuron per class were employed with the output encoding convention of a high level (0.9) from the output neuron corresponding to a given class and simultaneously low output (0.1) from other output neurons. Each neuron computes a log-sigmoid function of the weighted sum of its input. The updates of the weights and activation level parameters were carried out using the Levenberg-Marquardt optimization method for 100 epochs.

14.3.2.2 Clustering-Based Neural Network Classifier (CBNN)

Wang et al. (2008) developed a computationally efficient method based on neural network. This method is divided in two stages. In the first stage, the ISODATA algorithm is run on each training set to identify a number of clusters for each class. Each cluster center is labeled according to the class it belongs to and the entire set is used to build a Delaunay graph. In the second stage, a three-layered, feed-forward network is built as follows. For each pair of nodes belonging to different classes that are connected in the Delaunay graph, a neuron is created in the first hidden layer and its weight parameters are set to the coefficients of the hyperplane that separates the two clusters in question. A second layer of neurons is then added to perform the intersection of the half-spaces defined by the first layer to form the largest convex regions, each of which falls into a single class. Finally, the output layer joins the convex region into arbitrarily complex non-convex regions which define the decision region for each class.

It must be noted that the activation functions for all units are implicitly considered as hard limiters (or step functions) during the design stage. However, log-sigmoid functions may be used in the classification process. In the latter case a smoothing parameter is considered and the hard limiter results as a limiting process. More specifically, the sigmoid function is defined by

$$f(s) = \frac{1}{1 - e^{-s/\alpha}}$$

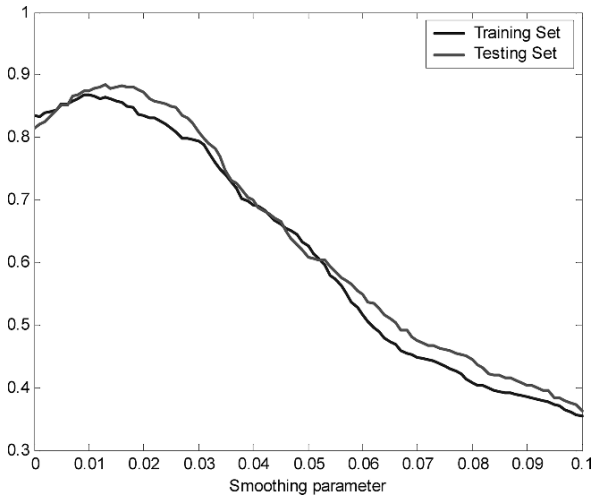


Fig. 14.1 Plot of kappa values against the smoothing factor. Optimum smoothing parameter is 0.015

where α is the smoothing parameter. As α approach to zero the plot of $f(s)$ tends to a hard limiter function.

Since different smoothing factors lead to different classification accuracies, a natural question to ask is how we can choose the best value for the smoothing parameter. In previous work, Silvan-Cárdenas (2003), α was empirically set to 0.02. In this study, we developed a scheme to choose the optimal parameter α with which the kappa value is at a maximum. The plot of the kappa value against α obtained for the data set of May is shown in Fig. 14.1. In this case, the optimum smoothing factor falls around 0.01. After several trials it was observed that the optimum α most likely lies at 0.015, which confirms that 0.02 is a good empirical choice. Another interesting observation is the fact that the optimum α based on the testing set (and still using the same trained network) reports a similar value as the optimum α based on the training set. This might indicate that (1) the training sample is representative of the classes under consideration and (2) the network can generalize very well the data that are not previously included in the training samples. Evidently, the second conclusion can be a consequence of the first one only if the training method succeeds.

This method was implemented in MATLAB software. The classifier is hereafter referred to as CBNN.

14.3.2.3 Maximum Likelihood Classifier (MLC)

For the purpose of evaluating the previous two types of neural network methods, we also adopted MLC as the third method. Equal *a priori* probability was assumed for all the classes in the implementation of MLC.

14.3.3 Results

To compare classification performance of the two images, spatially consistent training and test samples were prepared with the aid of two field surveys carried out in January and July 2004, close to the times of image acquisition. During both field surveys, an extensive number of GPS points were measured by a high precision Trimble GPS (Pathfinder Pro XRS receiver). The species type, percentage of surrounding vegetation as well as other tree inventory information such as DBH, crown area were recorded as well. Given the patchy distribution of mangrove species, we used polygon tools to define training and test samples on the images. In reference to the field collected GPS points, small polygons, each encompassing no more than 10 pixels, were delineated across the study area to serve as training and test samples. Special caution was made to only choose polygons that fall in pure stands of a specific species in order to avoid including mixed pixels. Two experiments were designed to assess the accuracy of each classification method given two different combinations of input bands: spectral bands only, or spectral and textural bands. The results were reported in detail below.

14.3.3.1 Classification Based on Spectral Information

In the first experiment, the four multispectral bands were employed as input bands while the panchromatic band was not taken into account. For each classifier the overall kappa value was computed using both the training and test sample sets to analyze its generalization characteristic. Intuitively, one should expect lower kappa values for the test set than for the training set. A kappa value based on the training set represents the ability of the model to fit the training data, however a kappa based on the test set reveals the capability of the model to generalize (i.e. achieve the correct classification of data not previously encountered). Therefore, the ratio of the later with respect to the former is an index of the level of generalization achieved by a supervised classifier, provided that the number of samples in both sets is sufficiently large for rigorous statistical comparison. The corresponding kappa values and generalization ratio for the tested classifiers are shown in Table 14.1b. Three results are clearly discernable. First, in general the CBNN and MLC classifiers performed better with the May image than with the February image, while the BP:24:12 classifier displayed lower accuracy with the May than February image. Second, The CBNN and MLC classifier considerably outperformed the BP:24:12 for the May image in terms of both the kappa value and the generalization ratio. The three classifiers achieved comparable accuracy when applied to the February image. Third, MLC yielded the highest generalization ratios (0.99 and 1.05) for both images.

User accuracy was derived for each classifier and land cover type (Table 14.1a). For the individual mangrove species, user accuracy ranged from 35.6% (for black mangrove in the May image with the BP:24:12 classifier) to 96% (for white mangrove in the May image with the CBNN classifier). The CBNN and MLC classifiers

Table 14.1 Accuracy of the three classification methods for the February and May IKONOS images using multispectral bands alone. (a) User accuracy for individual classes; (b) Kappa values from training and test samples, respectively, and ratios between two corresponding Kappa values

Land cover category	Feb-04			May-04		
	BP:24:12	CBNN	MLC	BP:24:12	CBNN	MLC
(a)	User's Accuracy (%)					
Red mangrove	88.8	81.6	86.6	44.3	94.3	92.6
White mangrove	56.8	65.6	73.3	82.1	96.0	92.4
Black mangrove	68.2	64.4	72.5	35.6	78.8	91.5
Gap	93.7	85.9	82.2	0.0	96.2	89.3
Lagoon	100.0	100.0	100.0	83.7	90.6	90.0
Rainforest	72.7	73.8	78.4	91.7	89.1	84.3
Road	94.6	100.0	89.9	90.4	98.0	71.8
(b)	Kappa Values					
Kappa (test samples)	0.74	0.73	0.78	0.49	0.87	0.86
Kappa (training samples)	0.79	0.78	0.79	0.6	0.87	0.83
Ratio	0.94	0.94	0.99	0.83	1.00	1.05

were noticeably more accurate than BP:24:12 when applied to either image, while in general, MLC gave consistently high user accuracy for the three mangroves in both images.

14.3.3.2 Classification Based on Textural and Spectral Information

As detailed above, the CBNN and MLC classifiers provided reasonably high overall classification accuracy when only spectral bands were considered. Given the high spatial detail associated with the panchromatic band of the IKONOS image, it was of interest to further investigate how well these two classifiers can utilize added textural information in assisting the classification process. In this experiment, the second order texture method, Grey Level Co-occurrence Matrix (GLCM), was adopted to extract the textural information from the panchromatic band of the IKONOS image. Displacement vectors at four directions (0, 45, 90, and 135 degrees), with a spatial distance of 1 pixel, were employed to compute three rotation invariant texture bands: Contrast (CON), Entropy (ENT), and Angular Second Moment (ASM) at three different window sizes: 9*9, 17*17, 25*25. The quantization level was set to 16 in all cases. Then, each texture band was resampled to the same resolution as the multispectral bands (4 m), and stacked together with the four multispectral bands as the input bands for the CBNN and MLC classifier. For the CBNN method, the smoothing parameter was fixed to 0.015. The respective kappa values based on the test samples are presented in Fig. 14.2.

The addition of textural bands to the multispectral bands significantly improved the classification results for both CBNN and MLC (Fig. 14.2). For the February

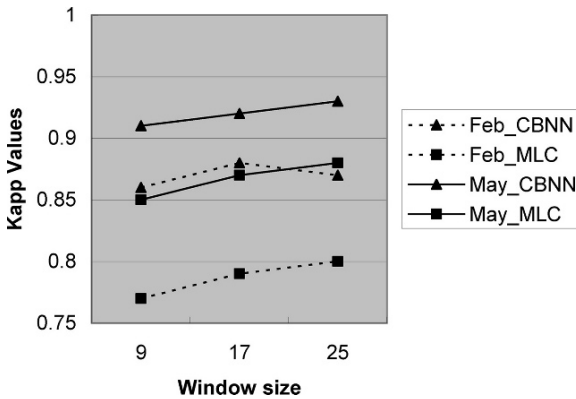


Fig. 14.2 Kappa values for the CBNN and MLC analyses of February and May images using both multispectral and textural bands. Feb_CBNN and Feb_MLC stand for CBNN and MLC methods applied to the February imagery. Similarly, May_CBNN and May_MLC stand for CBNN and MLC methods applied to the May imagery

image, the kappa values increased to 0.88 for CBNN and 0.8 for MLC, compared to 0.78 and 0.79, respectively when only multispectral bands are included. Likewise, for the May image, the kappa values when textural information was included were 0.93 for CBNN and 0.89 for MLC, compared to 0.87 and 0.83, respectively when textural information was not included. Furthermore, when textural information was included, analyses of the May image yielded consistently superior classification at all window sizes when compared to analyses of the February image. Finally, textural information extracted from a larger window size was more instructive than that from a smaller window size.

14.4 Spectral Discrimination Analysis of Mangrove Leaves with Lab Hyperspectral Remote Sensing

14.4.1 Data Collection and Preprocessing

Leaves of each species were sampled from trees growing in two different environmental settings: (1) areas supporting closed-canopy stands of large trees, some growing to more than 25 m, and (2) areas with a sparser cover of mostly short-stature (up to 3 m) trees that exhibited a wizened, shrub-like growth form. The former stands grow on organically rich soils of moderate salinity and relatively high nutrient availability, while the latter grow on sandy, coral reef-derived, soil that has lower nutrient concentrations, dries more rapidly between flood tides and rain storms, and is often higher in salinity (W. Sousa, unpublished data). A nutrient manipulation experiment conducted with *Rhizophora mangle* seedlings in this sandy

site demonstrated that their growth was nutrient-limited (L. Robinson, unpublished data). Leaves collected from the two sites differed in appearance and thickness: those from productive sites that support good growth tended to be larger, thinner, and more pliant than those collected from trees in the sandy site.

To determine whether the reflectance patterns of leaves from healthy individuals of the three mangrove species could be successfully discriminated, we selected 30 trees of each species for sampling from an array of productive stands across the study area. These ranged from fringe red mangrove stands growing at the water's edge to more inland stands dominated by white or black mangroves. Where possible, several trees of each species were sampled in each stand, so as to minimize the confounding influence of location on spectral measurements. Since leaves at different positions in the canopy might exhibit distinct spectral characteristics (due to differences in photosynthetic properties or water content), we stratified the leaf samples collected from each tree by height. From each tree, we collected one sample of 10 leaves from upper parts of the canopy surface and a second sample of 10 leaves from lower parts of the canopy surface. We were not able to sample leaves from the tops of taller trees at these productive sites, but the trees we sampled were growing in open areas, either at the water's edge or along a roadside, and therefore probably experienced similar levels of incident sunlight as the upper canopy of taller trees. Subsequent statistical analyses found that the reflectance patterns of leaves collected from upper versus lower heights in the canopy did not differ significantly for any of the three species (ANOVA, $P > 0.05$). Therefore, we used the pooled sample of 20 leaves to calculate each tree's mean reflectance curve.

To examine the effect of physiological stress and/or nutrient limitation on foliar spectral properties, we collected leaves from stunted individuals of each species that were growing in an area of sandy soils located approximately 100 m behind fringe red mangrove stands that border the back reef adjacent to the Galeta Marine Laboratory. We sampled leaves from 20 trees of each species, haphazardly selected from across an approximately 1 ha area of this vegetation type; a sample of 10 leaves was collected from each tree. Since the crowns of these small trees were easily reached and contained relatively few leaves, we collected from the entire canopy of each tree; no effort was made to stratify these samples by height.

All leaves were collected on 16 July, 2004. They were immediately sealed in plastic bags, kept in a dark cooler, and transported back to the nearby laboratory for analysis. Leaf reflectance was measured with a Field Spec Pro FR (Analytical Spectral Devices, Boulder, CO, USA). The measurement procedure followed that employed by Pu et al. (2003). The light source consisted of two 500W halogen tungsten filament lamps. All spectra were measured in reflectance mode at the nadir direction of the radiometer with a 25° FOV. A white Spectralon panel was employed as the white reference and measured every five minutes to convert leaf radiance to percent reflectance. The spectrometer was configured to yield a spectra with 25 spectral averaging. Each sample of ten leaves was stacked in an overlapping pile on top of a calibrated black cloth and care was taken to make sure the field of view was fully occupied by leave stacks. The adaxial surfaces of a sample were measured five times, from which an average spectral reflectance curve was generated. Spectral

reflectance was originally measured over the ranges of 350–1000 nm at 1.4 nm intervals and 1000–2500 nm at 2.2 nm intervals. The entire spectral range (350–2500 nm) was automatically resampled to 1 nm when exported to the computer. To reduce system noise and redundancy between adjacent bands, we computed an average reflectance for each 10 nm interval, providing a total of 215 wavebands for analysis.

For band selection and classification of leaves from healthy trees, we had a sample size of 30 spectra for each tree species. We randomly split these 30 samples into a training group comprised of 20 samples and a test group of 10 samples; the latter were used to assess our classification accuracy. This procedure was repeated 10 times on randomly drawn sets of training and test samples.

14.4.2 Band Selection and Tree Species Classification

Due to the high correlation inherent to adjacent wavebands, it was neither efficient nor reliable to include all 215 measured bands in the classification at one time. Instead, one must first choose a subset of bands that will maximize the likelihood of discrimination before proceeding with a conventional classification. A number of band or feature selection methods have been developed and documented in the remote sensing literature, including Principal Component Analysis (PCA), Fisher's Linear Discriminant Analysis (LDA), Penalized Discriminant Analysis (PDA), and wavelet-based feature selection (Yu et al. 1999, Pu and Gong 2004). Among them, LDA is the procedure that has been most widely adopted. However, a critical problem associated with LDA is that it will not provide a reliable solution when reflectance values for many highly correlated wavebands are included in the analysis and the number of available training samples is small. In this circumstance, estimates of within-class covariance matrices from the training samples are poor and unstable. In this study, we had 215 bands of reflectance values while only 20 samples for each species as training samples. The results of an LDA on such data would be highly questionable; the projection axis is likely to be misoriented, giving rise to over-fitting: i.e. a perfect performance on the training data, but a poor performance on the test data. Yu et al. (1999) provide a good graphical illustration of the problem.

To circumvent this problem, a method was developed by Wang and Sousa (2008) by first applying a series of one-way ANOVAs to filter out wavebands that did not differ significantly in mean reflectance among leaves of the three tree species. A one-way ANOVA, with species as the independent factor, was carried out for each of the 215 wavebands. The resultant probability provided an index of the importance of the tested band to the discrimination of the tree species. We considered $P \leq 0.01$ as an indication that the mean reflectance of at least two of the three species differed in the tested band; all bands meeting this criterion were included in the LDA. One potential criticism of this band selection procedure is that the results of tests on adjacent bands are not statistically independent. However, our objective in applying ANOVA was not to test hypotheses about differences within specific bands; rather, we were seeking to eliminate bands from the analysis that provided no useful information

for discriminating species' reflectance patterns, and thereby reduce the number of analyzed bands to a level that would be operational for LDA. This band selection procedure was performed on all the training samples.

An LDA was then performed using the wavebands that ANOVA identified from the above procedure. The principle of LDA is to project the original redundant data to a new orthogonal space oriented along the axis that can maximize the ratio of between-class to within-class variance matrices of the training samples. The axis of the new space is aligned in the order of discrimination power among groups such that the first axis provides the greatest overall discrimination, the second provides second greatest, and so on. If we denote the total number of groups to be classified as NG and the total number of original bands as NB, then the number of dimensions for the new space is equal to either NG-1 or NB, whichever is smaller. Since in practice, NB is usually larger than NG, LDA will typically yield a new data set with NG-1 dimensions. In this way, the data dimensions are significantly reduced.

The significance of a specific wavelength to a discrimination function can be determined by examining the standardized coefficients for that band. The interpretation of the standardized coefficients resembles the logic of multiple regressions. The larger the absolute value of standardized coefficient, the larger is the respective variable's unique contribution to the discrimination as specified by the respective discriminant function. As such, by ordering the standardized coefficients the optimal wavebands were determined.

Given the fact that we have three species to classify, LDA generated two discriminant functions, with which the test samples were transformed. Then a Mahalanobis distance classifier was performed. A kappa value was calculated to assess the classification accuracy (Cohen 1960).

14.4.3 Discrimination Between Leaves from Healthy Versus Stressed Trees

Previous studies have found that leaf spectral reflectance increases in portions of the visible and very-near infrared range (but not in the infrared) as a plant experiences physiological stress (Carter 1993, 1994, Carter and Knapp 2001). This response has been documented for numerous plant species when subjected to various agents of stress. We therefore focused on the 400–800 nm waveband in our comparison of healthy and stressed leaves. The sensitivity of reflectance to stress (i.e. relative change in reflectance) varies considerably within this spectral range. Sensitivity is greatest for wavelengths (e.g. 605, 695, and 710 nm) at which absorption by chlorophylls *a* and *b* is relatively weak. At these wavelengths, even a slight drop in leaf chlorophyll content caused by stress results in a large increase in leaf reflectance (Carter 1993).

As demonstrated by Carter (1994), reflectance sensitivity is best expressed as a ratio of reflectance in a stress-sensitive band to reflectance in a stress insensitive band. For our study, we calculated four narrow band leaf reflectance ratios

as indices of stress: R695/R420, R605/R760, R695/R760, and R710/R760. Carter (1994) found these ratios to be particularly sensitive indicators of stresses that affect chlorophyll content. We used ANOVA to compare the means of these ratios between leaf samples from trees growing in productive and stressful sites.

14.4.4 Results

14.4.4.1 Band Selection and Classification

Figure 14.3 presents the mean reflectance spectra of leaves from the three mangrove species; values for healthy and stressed trees are plotted separately (Fig. 14.3). We will first examine patterns of reflectance for leaves from healthy trees growing in productive sites. As expected, the general shapes of the species' curves are very similar, with considerable overlap.

However, one-way ANOVA tests revealed significant heterogeneity among the species in particular wavebands. Of the 215 10 nm-wide wavebands tested, 116 bands exhibited significant ($P \leq 0.01$) interspecific variation in mean reflectance. These bands were clustered in five areas of the spectrum, i.e. 350–510 nm, 610–690 nm, 760–810 nm, 1370–1550 nm, and 1850–2500 nm. Bands within each of these areas are highly correlated and cannot be treated as independent estimates of species-level response. To reduce this correlation, we first regrouped the 116 significant bands into three regions as follows – region 1: VNIR (350–510 nm, 610–690 nm, and 760–810 nm); region 2: SWIR I (1370–1550 nm); and region 3: SWIR II (1850–2500 nm). An LDA was executed separately within each region and the standardized coefficients for two discrimination functions were respectively calculated and ranked. We concluded that a band was influential for its particular region if the absolute value of its LDA standardized coefficients were ranked among the top ten for both discrimination functions. Table 14.2 lists such influential bands for each region of wavelengths considered in the analysis.

The final classification of mangrove species was generated by LDA after pooling the influential bands from each region. In both the training and test samples, leaves of the three mangrove species were well separated in discriminant space. The average kappa value for the ten sets of test samples was 0.9, with a range of 0.85 to 1.00. This indicates that our method for extracting influential wavebands from the hyperspectral data, in combination with an LDA-based classification procedure, was very successful in discriminating the leaves of different mangrove species. Our results concur with several other researches that achieved good discrimination through use of the LDA method (Gong et al. 1997, Van Aardt and Wynne 2001, Clark et al. 2005). In addition, the LDA results show that the first discriminant function alone is sufficient to distinguish red from either black or white mangrove leaves. Examination of the standardized coefficients associated with the first discriminant function reveals that reflectance at the 780, 790, 800, 1480, 1530, and 1550 nm wavebands contribute most strongly to the first discriminant function. In other words, these

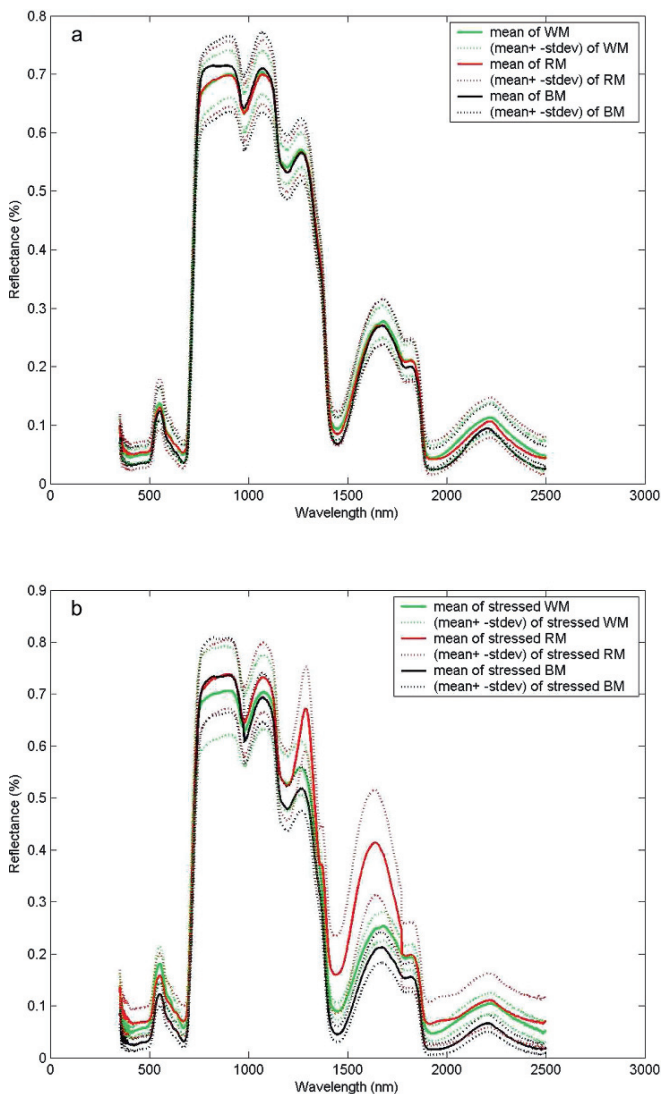


Fig. 14.3 (a) mean and (mean \pm 1 stdev) reflectance spectra for leaves from healthy leaves of the three mangrove species (WM: White Mangrove; RM: Red Mangrove; BM: Black Mangrove); (b) mean and (mean \pm 1 stdev) reflectance spectra for leaves from physiologically stressed leaves of the three mangrove species

bands are critical to the discrimination of red from the other two types of mangrove. The second discriminant function best distinguishes white from black mangrove leaves; this function was most strongly influenced by wavebands at 770, 780, 790, 800, 1430, and 1480 nm.

Table 14.2 Results of one-way ANOVA showing the potentially important wavelengths for discriminating leaf samples from healthy trees of the three mangrove species

Spectral region	Region 1: VNIR [350–510, 610–690, 760–810] (nm)	Region 2: SWIR I [1370–1550] (nm)	Region 3: SWIR II [1850–2500] (nm)
Influential wavelengths in each region	490, 500, 630, 770, 780, 790, 800	1400, 1430, 1480, 1530, 1550	1940, 1970, 1990

14.4.4.2 Discrimination Between Leaves from Healthy Versus Stressed Trees

One or more of the four reflectance ratio indices proved useful in detecting stress in each of the mangrove species (Table 14.3). R605/R760, R695/R760, and R710/R760 were effective in distinguishing stressed from non-stressed red mangrove leaves. In the case of white mangrove, R695/R420 was the only ratio that successfully detected the presence of stress. All four ratios were capable of detecting stress in black mangroves.

Table 14.3 Results of ANOVA. Entries are *P* values by comparing the mean values of the four narrow band ratios between stressed and healthy leaves; bolded values are considered statistically significant (*P* value < 0.01)

Narrow Band Ratios	Mangrove species		
	Red	White	Black
R695/R420	0.371	< 0.001	< 0.001
R605/R760	0.009	0.799	< 0.001
R695/R760	0.008	0.888	< 0.001
R710/R760	0.013	0.613	< 0.001

14.5 Conclusion

Multitemporal information can be very helpful in discriminating the canopies of different forest species (Jensen 2004). Our results confirmed that multiseasonal imagery can aid species-level classification of mangrove forests. Our study found that an IKONOS image acquired during the early rainy season more effectively captured the difference among mangrove species than one taken during the dry season. This difference is probably attributable to phenological and physiological changes that affect the reflectance of tree canopies. At our study sites, mangroves flush new leaves during the early wet season, while they experience stress from drought and high soil salinity during the dry season.

When only multispectral bands were included in the classification, MLC proved the best method for discriminating different mangrove species, consistent with the

findings of other studies, mentioned above. CBNN demonstrated a similar performance but at the cost of a considerable increment in computing time. However, when textural information was added to the classification, CBNN exhibited a strong advantage over MLC in characterizing the complex decision boundary associated with the combination of textural and spectral bands. The relative loss in MLC's power of discrimination when textural information was incorporated could have resulted from a violation of its central assumption of a multivariate Gaussian distribution model, as discussed earlier. Neural network-based analyses do not rest on this assumption, and thus gained discrimination power from the added textural information. Compared to the traditional back-propagation neural network method, the new CBNN method provides a computational simpler yet effective way in discriminating different mangrove species.

The high classification accuracy we obtained with the leave-level hyperspectral reflectance confirms the great potential of using hyperspectral data to distinguish mangrove species. We are confident that the use of narrow band hyperspectral data can effectively overcome the problem of overlap in spectral characteristics among species observed in our previous analyses of wide band multispectral imagery (Wang et al. 2004 a,b).

Acknowledgement Ms. Jose Silvan is thanked for his assistance in implementing CBNN method. This study was supported by grants to Le Wang from the National Science Foundation (DEB-0614040, DEB-0810933), from the Texas Remote Sensing Consortium and Texas State University research enhancement program, and financial support from University at Buffalo, and by grants to Wayne P. Sousa from the National Science Foundation (DEB-0108146) and the U.C. Berkeley Committee for Research.

References

- Alongi DM (2002) Present state and future of the world's mangrove forests. *Environ Conserv* 29:331–349
- Carter GA (1993) Response of leaf spectral reflectance to plant stress. *Am J Bot* 80:239–243
- Carter GA (1994) Ratios of leaf reflectance in narrow wavebands as indicators of plant stress. *Int J Remote Sens* 3:697–703
- Carter GA, Knapp AK (2001) Leaf optical properties in higher plants: linking spectral characteristics to stress and Chlorophyll concentration. *Am J Bot* 4:677–684
- Carter GA, Paliwal K, Pathre U, Green TH, Mitchell RJ, Gjerstad DH (1989) Effect of competition and leaf age on visible and infrared reflectance in pine foliage. *Plant Cell Environ* 12:309–315
- Clark ML, Roberts DA, Clark DB (2005) Hyperspectral discrimination of tropical rain forest tree species at leaf to crown scales. *Remote Sens Environ* 3–4:375–398
- Cohen J (1960) A coefficient of agreement of nominal scales. *Educ Psychol Meas* 20:37–46
- Cubit JD, Thompson RC, Caffey HM, Windsor DM (1988) Hydrographic and meteorological studies of a Caribbean fringing reef at Punta Galeta, Panama: hourly and daily variations for 1977–1985. *Smithsonian Contributions in Marine. Science* 32:1–220
- Cubit JD, Caffey HM, Thompson RC, Windsor DM (1989) Meteorology and hydrography of a shoaling reef flat on the Caribbean coast of Panama. *Coral Reefs* 8:59–66
- Duke NC, Pinzón MZS (1993) Mangrove forests. In: Keller BD, Jackson JBC (eds) Long-term assessment of the oil spill at Bahía Las Minas, Panama, synthesis report, vol 2. Technical report.

- OCS Study MMS 93-0048. U.S. Department of the Interior, Minerals Management Service, Gulf of Mexico OCS Region, New Orleans, Louisiana, pp 447–533
- Duke NC, Pinzón MZS, Prada MC (1997) Large-scale damage to mangrove forests following two large oil spills in Panama. *Biotropica* 29:2–14
- Ellison AM, Farnsworth EJ (1996) Anthropogenic disturbance of Caribbean mangrove ecosystems: past impacts, present trends, and future predictions. *Biotropica* 4:549–565
- Ellison AM, Farnsworth EJ (2001) Mangrove communities. In: Bertness MD, Gaines SD, Hay ME (eds) *Marine Community Ecology*. Sinauer Associates, Sunderland, MA, pp 423–442
- Farnsworth EJ, Ellison AM (1997) The global conservation status of mangroves. *Ambio* 26: 328–334
- FAO (2003) *State of the world's forests*. Report of the Food and Agriculture Organization of the United Nations, Rome
- Gao J (1998) A hybrid method toward accurate mapping of mangroves in a marginal habitat from Spot multispectral data. *Int J Remote Sens* 10:1887–1899
- Gao J (1999) A comparative study on spatial and spectral resolutions of satellite data in mapping mangrove forests. *Int J Remote Sens* 14:2823–2833
- Gong P, Pu RL, Yu B (1997) Conifer species recognition: an exploratory analysis of in situ hyperspectral data. *Remote Sens Environ* 2:189–200
- Green EP, Clark CD, Mumby PJ, Edwards AJ, Ellis AC (1998) Remote sensing techniques for mangrove mapping. *Int J Remote Sens* 5:935–956
- Held A, Ticehurst C, Lymburner L, Williams N (2003) High resolution mapping of tropical mangrove ecosystems using hyperspectral and radar remote sensing. *Int J Remote Sens* 24: 2739–2759
- Hogarth PJ (1999) *The biology of mangroves*. Oxford University Press, Oxford, UK
- Hutchings P, Saenger P (1987) *The ecology of mangroves*. University of Queensland Press, St. Lucia, Australia
- Jensen JR (2004) *Introductory digital image processing: a remote sensing perspective*, 3rd edn. Prentice Hall, Upper Saddle River, NJ, USA
- Kathiresan K, Bingham BL (2001) Biology of mangroves and mangrove ecosystems. *Adv Mar Biol* 40:81–521
- Lugo AE, Snedaker SC (1974) The ecology of mangroves. *Annu Rev Ecol Syst* 5:39–64
- Mumby PJ, Edwards AJ (2002) Mapping marine environments with IKONOS imagery: enhanced spatial resolution can deliver greater thematic accuracy. *Remote Sens Environ* 2–3:248–257
- Pu R, Ge S, Kelly NM, Gong P (2003) Spectral absorption features as indicators of water status in coast live Oak (*Quercus agrifolia*) leaves. *Int J Remote Sens* 9:1799–1810
- Pu RL, Gong P (2004) Wavelet transform applied to EO-1 hyperspectral data for forest LAI and crown closure mapping. *Remote Sens Environ* 2:212–224
- Rasolofoharinoro M, Blasco F, Bellan MF, Aizpuru M, Gauquelin T, Denis J (1998) A remote sensing based methodology for mangrove studies in Madagascar. *Int J Remote Sens* 10: 1873–1886
- Rumelhart DE, Hinton GE, Williams RJ (1986) Learning representations by back-propagating errors. *Nature* 323:533–536
- Saenger P, Hegerl EJ, Davie JDS (1983) Global status of mangrove ecosystems. *Environmentalist* 3:1–88
- Silvan-Cárdenas JL (2003) Optimal design of neural networks for land-cover classification from multispectral imagery. In: Bruzzone L (ed) *Proc. SPIE (Image and Signal Processing for Remote Sensing IX)*, 5238, pp 420–431
- Tomlinson PB (1986) *The botany of mangroves*. Cambridge University Press, Cambridge, UK
- Van Aardt JAN, Wynne RH (2001) Spectral separability among six southern tree species. *Photogramm Eng Rem S* 12:1367–1375
- Venkataratnam L, Thammappa SS (1993) Mapping and monitoring areas under prawn farming. *Interface: A Bulletin from the NRSA Data Centre* 4:4–7
- Wang L, Silvan J, Sousa WP (2008) Neural network classification of mangrove species from multiseasonal IKONOS imagery. *Photogramm Eng Rem S*. (In press)

- Wang L, Sousa WP (2008) Distinguishing mangrove species with laboratory measurements of hyperspectral leaf reflectance. *Int J Remote Sens.* (In press)
- Wang L, Sousa WP, Gong P (2004a) Integration of object-based and pixel-based classification for mapping mangroves with IKONOS imagery. *Int J Remote Sens* 24:5655–5668
- Wang L, Sousa WP, Gong P, Biging GS (2004b) Comparison of IKONOS and Quickbird images for mapping mangrove species on the Caribbean Coast of Panama. *Remote Sens Environ* 91: 432–440
- Yu B, Ostland IM, Gong P, Pu RL (1999) Penalized discriminant analysis of in situ hyperspectral data for conifer species recognition. *IEEE T Geosci Remote* 5:2569–2577